Engineered Science

RESEARCH PAPER View Article Online

Surface Modifications of Superparamagnetic Iron Oxide Nanoparticles with Polylactic Acid-Polyethylene Glycol Diblock Copolymer and Graphene Oxide for a Protein Delivery Vehicle

Linh Doan,[1,2] Yang Lu,[3] Megha Karatela,[1] Vu Phan,[1] Clayton Jeffryes,[1,4*] Tracy Benson[1,2*] and Evan K. Wujcik[1,3*]

As a protein delivery vehicle, superparamagnetic iron oxide nanoparticles (SPION) with an average size of 19.6 ± 4.8 nm were coated with polylactic acid (PLA) (5000)-polyethylene glycol (PEG) (10000) diblock copolymer and single layer graphene oxide (GO). Bovine serum albumin was selected as the model protein, and the drug loading capacity of the designed vehicle is 2013 ± 79 mg g^{-1}. The drug release result shows that the average percentage of cumulative drug release after 47 days in vitro is 37.7% ± 1.4%.

Keywords: Super paramagnetic iron oxide nanoparticles; Graphene oxide; Diblock co-polymer

Received 18 December 2018**, Accepted** 24 April 2019

DOI: 10.30919/es8d510

1. Introduction

Today, even with great advances in cancer treatments such as surgery, radiotherapy, and chemotherapy, cancer is still one of the deadliest threats to human health.[1,2] Chemotherapy and radiotherapy, which depend heavily on anticancer drugs, can have negative side effects on the cardiovascular, digestive, and respiratory system.[3,4] Hence, delivering a minimum quantity of total drug to patients, while maximizing delivery to targeted tissues, is of great importance.

SPIONs have many applications in the biomedical industry. For example, iron oxide nanoparticles are used as T2 contrast agents due to their predominant T2-relaxation effects, giving rise to signal reduction on T2-weighted images.[5] The recently demonstrated use of bio-vectorized particles for target-specific imaging creates the possibility for MRI molecular probes.[7] Moreover, SPIONs have superparamagnetism that can be controlled by an external magnetic field, which can enable guided drug delivery to targeted areas in the human body.[8] By doing so, the dosage of medication can be decreased and the side effects of the medicine can be kept to a minimum.[1] SPIONs can also be applied to in vitro applications such as genetics research, and other biomedical technologies based on immune magnetic separation of cells, proteins, deoxyribonucleic acid/ ribonucleic acid (DNA/RNA), bacteria, virus, and other biomolecules.[1]

SPIONs can be produced by the co-precipitation, microemulsion, hydrothermal synthesis, and high temperature decomposition methods.[6] The co-precipitation method was used in this study which produced primarily magnetite.[9] In this method, the transformation of magnetite to maghemite can be suppressed.[9] Another advantage is the rapid and high yield of magnetite.[6] However, this method has a weak control of the nanoparticle size distribution due to the influence of kinetic factors on nucleation and growth of the crystals, despite the high concentration of nanoparticles per batch.[9] Another disadvantage is the oxidation and aggregation of SPIONs,[6] factors that can be minimized by ultrasonication and coating immediately following synthesis.

Hydrophobic SPIONs tend to undergo opsonization and are typically cleared immediately by the mononuclear phagocytic system (MPS).[6] However, SPIONs can be easily coated with polyethylene glycol (PEG). PEG is soluble in water, and organic solvents such as toluene, and chloroform, and it increases the solubility of other large molecules irrespective of their size.[10] PEG is widely used as a coating material for nanoparticles due to the following properties: easy excretion through the kidney, low interfacial free energy with water, excluded volume effect, nonimmunogenic, and nonantigenic properties.[11] PEG coatings suppress platelet adhesion, reducing risk of thrombus formation, tissue damage, and other cytotoxic effect in vitro and in vivo.[10] PEG does not negatively impact (i.e. protein modification, loss of function or active sites, mutations) active protein or cells even though PEG interacts with some of them directly.[10] By having a hydrophilic coating on the SPIONs, the in vivo circulation increases because the interaction of the SPIONs with the plasma proteins is avoided, reducing the uptake by the MPS.[6] Once the SPIONs are coated with PEG, the PEG acts as a good spacer for the attachment of different biomolecules.[6] Basically, PEG-coated surfaces become hydrophilic and protein rejecting.[10] In this study, PLA-PEG is selected to coat SPION.

Graphene is a one-atom thick sheet of carbon.[12] Graphene and graphene oxide (GO) have previously been used for biocompatible

[1]*Dan F. Smith Department of Chemical Engineering, Lamar University, Beaumont, TX, USA*
[2]*OPERANDO Spectroscopy Laboratory, Dan F. Smith Department of Chemical Engineering, Lamar University, Beaumont, TX, USA*
[3]*Materials Engineering And Nanosensor (MEAN) Laboratory, Department of Chemical and Biological Engineering, The University of Alabama, Tuscaloosa, AL, USA*
[4]*Nanobiomaterials and Bioprocessing (NAB) Laboratory, Dan F. Smith Department of Chemical Engineering, Lamar University, Beaumont, TX, USA*
***E-mail:** tracy.benson@lamar.edu; cjeffryes@lamar.edu; Evan.Wujcik@ua.edu*

(materials that do not cause any inflammation or damage to the variety of cells due to non-toxicity)[13] implantable[14] applications. GO is oxidized graphene[15] with surface epoxy and carboxyl groups.[12] The oxygen-containing function groups in GO give it hydrophilic properties due to enhanced hydrogen bonding.[12] This hydrophilicity enables biomolecule deposition within GO scaffolds.[15]

PLA-PEG molecules can be attached onto graphene oxide by covalently binding suitable PLA-PEG derivatives on the GO molecules. Another way involves using the functional groups attached to the GO, or attaching amphiphilic PEG copolymers, such as pluronics or poloxamers.[15] These functional groups are created by strong oxidation and are distributed randomly on the basal planes and the edges of the graphene oxide sheets, oxidizing aromatic rings to generate aliphatic regions (sp_3 the sp_2 hybridized matrix).[16] In this study, GO is deposited on the outer layer of PLA-PEG, creating a large surface area material with a high concentration of functional groups, enabling high drug-loading.[16]

This newly designed drug delivery vehicle will allow loading of high molecular weight drugs that cannot be loaded into other core-shell particles such as SPIONs-mesoporous silica. This drug delivery vehicle also has the potential to load two different types of drugs, is easy to synthesize, and is low-cost.

2. Experimental Section

Materials:

Iron (III) chloride hexahydrate, iron (II) chloride tetrahydrate, ammonium hydroxide solution (28 wt% NH_3 in H_2O), and tetrahydrofuran were purchased from Sigma Aldrich. Hydrochloric acid was purchased from Fisher Scientific. Single layer graphene oxide was purchased from Cheap Tube Inc. PEG(10000)-b-PLA(5000) diblock polymer was purchased from Polymersciences. All materials were used as received.

Synthesis of SPIONs:

SPIONs were synthesized by the co-precipitation method previously described.[17] First, 500 ml of 0.7 M NH_4OH was prepared and poured into a two-necked round bottom flask and N_2 was bubbled through the solution while stirring. Next, 10.81 g of $FeCl_3{\cdot}6H_2O$ was dissolved in 40 ml of DI water and 3.97 g of $FeCl_2{\cdot}4H_2O$ was dissolved in 10 ml 2 M HCl. The two iron solutions were then mixed together and the entire 50 ml was added drop-wise to the flask containing NH_4OH solution. Stirring was reduced when the mixture turned black. The reaction continued for 30 minutes in an N_2 atmosphere. The particles were collected at the bottom of the flask using a neodymium magnet and the supernatant was removed and replaced with DI water.

Surface Modification of SPION with PLA-PEG:

This study used emulsion polymerization to coat PLA-PEG on SPION particles. 108 mg of PLA-PEG was mixed with 6–30 mg of SPION, 20 ml of THF, and 15 ml DI water. Then, the mixture was sonicated for 2 h, stirred, centrifuged at 3000 rpm for 5 minutes, and heated at 40 °C until the THF was evaporated. After drying, the total volume was adjusted to 15 ml with DI water. The mixture was then centrifuged and the supernatant was decanted. The product of PLA-PEG coated SPION was kept for further modifications.

Preparation of SPION/PLA-PEG/GO:

Based on the method of Angelopoulou *et al*. (2015),[16] 300 mg of Graphene Oxide (GO) was mixed with 1500 ml DI water, which gave a concentration of 0.2 mg ml^{-1}, was sonicated for 2 h. Then, 272.5 ml of GO-DI was mixed with SPION/PLA-PEG, which was made in the previous step. This gave the ratio of 50/50 wt% of GO/PLA-PEG. The GO/PLA-PEG ratio, the molecular weight of the PLA-PEG is based on Angelopoulou *et al*. study.[16] The mixture was then bath sonicated for 2 h. Then, the mixture was centrifuged at 1116×*g* for 5 min. The supernatant of the mixture was then bath sonicated for 1 h.

Loading of the delivery vehicle:

In this study, all of the experiments were performed in triplicate, and all of the error bars (calculated using standard deviation) are shown in the figures. Error bars shown as one standard deviation, except where otherwise stated.

The SPION/PLA-PEG/GO solution was then dried completely at 80 °C. The weight of SPION/PLA-PEG/GO was measured. Then, the product was divided into three equal aliquots. Next, 1 g of bovine serum albumin (BSA) was dissolved in 10 ml DI water and 3 ml of stock BSA solution was mixed with 27 ml DI water, which gave a concentration of 10 mg BSA ml^{-1}. In order to remove the impurities, the mixture was then centrifuged at 500 rpm for 5–10 minutes. The supernatant was removed and equally divided into three vials. The volume of BSA in each vial was measured then mixed with 1 vial of dried SPION/PLA-PEG/GO.[18] After extraction, SPION/PLA-PEG/GO was recovered from the suspension using a Neodymium magnet. This extraction process recovered BSA loaded SPION/PLA-PEG/GO nanoparticles, and BSA non-loaded SPION/PLA-PEG/GO nanoparticles. 1 ml of the supernatant was sampled, and the absorbance measured using spectrophotometry at 280 nm, 278 nm, and 260 nm every 10 minutes.

The loading amount (Q, mg BSA (g Fe_3O_4/PLA-PEG/GO)$^{-1}$) was calculated by following equation[18]:

$$Q = \frac{(C_0 - C)V}{m} \quad (1)$$

where C_0 and C are the initial concentration and concentration at time, *t* (min), of BSA in solution (mg BSA ml^{-1}), V is the reaction volume (ml), and m is the mass of Fe_3O_4/PLA-PEG/GO (g). The C_0, m, and V in this study are 10 mg ml^{-1}, 0.059 g, and 10 ml, respectively.

The concentration of BSA in the solution can be roughly estimated by the following equation:

$$C = 1.55 \times A_{280} - 0.76 \times A_{260} \quad (2)$$

where A_{280} and A_{260} are the spectrophotometric absorbances at 280 nm and 260 nm, respectively.

The drug loading capacity (%DL) was calculated by the following equation:[19]

$$\%DL = \frac{Weight\ of\ BSA\ absorped\ on\ to\ the\ nanoparticles(mg)}{Weight\ of\ \ nanoparticles(mg)} \times 100 \quad (3)$$

The entrapment efficiency (%EE) was calculated by the following equation: [19]

$$\%EE = 100 \times \frac{Weight\ of\ BSA\ absorped\ on\ to\ the\ nanoparticles(mg)}{Weight\ of\ \ nanoparticles(mg)} \quad (4)$$

BSA release the delivery vehicle:

Each of the magnet-collected BSA-loaded SPION/PLA-PEG/GO samples was mixed with 11 ml of 0.002 M Phosphate Buffer Saline (PBS) in a 15 ml centrifuge tube. Then, the centrifuge tube was incubated in a water bath at 37 °C and agitated for 10 minutes every 12 h. Every 24 hours, after agitation, the centrifuge tube was centrifuged at 400×*g* for 18 minutes. Then, 4 ml of solution was removed from the centrifuge

tube and placed in a vial. Then, 4 ml of pure PBS was put in the centrifuge tube to replace the sampled volume. After 34 days, all of the samples were analyzed by UV-vis spectrophotometry at 280 nm and 260 nm.

The amount of BSA released was calculated using the following equations:

Mass of the BSA in solution:

$$m_{t,i}=C_i\times V_t \tag{5}$$

where $m_{t,i}$, C_i, and V_t are the total mass of the BSA in solution at the time of sampling aliquot i (mg), the concentration of BSA in the sampled aliquot i (mg ml^{-1}) and total volume of the solution in the tube (ml), respectively. In this study, V_t = 11 ml and the volume aliquot removed for spectrophotometry was V_s = 4 ml.

The mass of the BSA in the liquid phase in the tube after sampling, $m_{t,i+}$, was calculated by:

$$m_{t,i+}= C_i\times(V_t-V_s)=m_{t,i}-C_iV_s \tag{6}$$

The mass released between removing samples i and $i+1$ was therefore:

$$m_{d,i}=m_{t,i+1}-m_{t,i+}+C_iV_s \tag{7}$$

where $m_{d,i}$ is the amount of BSA released during day i.

Cumulative drug release is therefore:

$$Cum_n=\sum_{i=0}^{i=n} m_{d,i} \tag{8}$$

where Cum_n is the total BSA released (mg) between t = 0 and day n.

The percentage cumulative drug release was calculated by:

$$PCDRR_n=\frac{Cum_n}{M_{DL}}\times 100 \tag{9}$$

where $PCDRR_n$ and m_{DL} are the percentage cumulative drug release (%) on day n and mass of BSA loaded on the NPs (mg), respectively. In this study, m_{DL} = 110 mg.

Scanning Electron Microscope (SEM) measurements:

The morphology of the nanoparticles was characterized with an SEM (JEOL 6500). The operating conditions were: accelerating voltage 5 kV, and probe current 20 pA. The dried samples were placed on the aluminum stub. ImageJ software was used to calculate the SPIONs diameter distribution from the SEM images.[20]

Fourier Transform Infrared Spectroscopy (FTIR) analysis:

All of the samples were dried, ground, and pressed in KBr disks before analyzed by a Tensor 27 FTIR spectrometer coupled with a Hyperion 1000 ATR microscope accessory, which were bought from Bruker Optics, Inc.

3. Results and Discussion

The SEM and FTIR confirmed the bonding of SPION with PLA-PEG and GO. Moreover, the SEM images clearly show adsorption of BSA to the surface of the SPIONs and FTIR confirms bonding of PLA-PEG and GO to the SPIONs. Taken together, these results imply the successful construction of the SPION/PLA-PEG/GO material with considerable surface loading of BSA.

3.1. Characterization of the Delivery Vehicle

SEM and FTIR were used to observe and confirm the bonding of protein to SPION/PLA-PEG/GO on the delivery vehicle.

3.1.1. SEM Measurements

SEM images of the SPION materials are presented in Fig. 1. As seen in Fig. 1a, SPION is agglomerated after synthesis. In this study, agglomeration can be avoided by using an ultra-sonic bath.

As seen in Fig. 1b, the SPION particles are much smaller compared to the PLA-PEG polymer. However, at 10 μm, Fig. 1b shows clearly

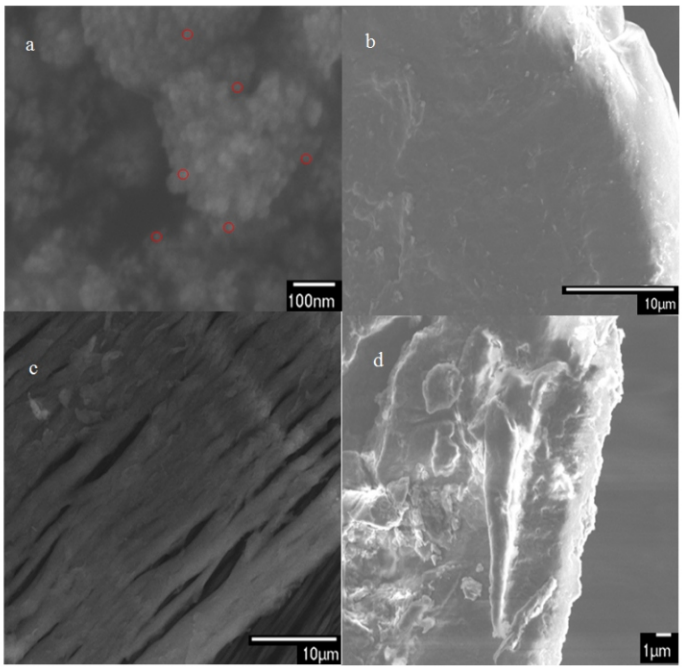

Fig. 1 SEM images a) SPION, b) SPION coated with PLA-PEG, c) SPION coated with PLA-PEG and GO, d) SPION coated with PLA-PEG with BSA attached to GO.

SPION particles were attached to the polymer, which later was supported and confirmed by FTIR (vide infra).

As seen in Fig. 1c the SPION particle was still attached to the PLA-PEG. However, the SEM can't take an image which shows the GO outside of the PLA-PEG due to the reaction between electron beam and the protein delivery vehicle.

Similar to Fig. 1c, the electron beam reacts with the protein delivery vehicle, GO was not shown in Fig. 1d. However, the reaction rate of electron beam and the protein delivery vehicle was slowed down.

The SPION particle size distribution is presented in Fig. 2. Most particles have a diameter ranging from 15 to 25 nm with an average diameter of 20 ± 5 nm (1σ).

3.1.2. FTIR

The FTIR spectra of the SPION, diblock copolymer, and vehicle are shown in Fig. 3. FTIR is an effective instrument to quantitate the structure on the functional groups in nanoparticles. This measurement was used to determine the functional groups, which in turn confirms the final structure of the drug delivery vehicle.

As seen in Fig. 3, for SPION/PLA-PEG/GO ratio 1:2 (wt/wt) spectra, the peak at 1751 cm^{-1} shows the stretching frequencies for C=O which matches GO and PLA-PEG spectra. Moreover, all of the peaks from 500 cm^{-1} to 2500 cm^{-1} match the PEG-PLA spectra. At 3410 cm^{-1}, SPION/PLA-PEG/GO ratio 1:2 (w/w) peak matches the peak of GO at 3426 cm^{-1} and the peak of SPION at 3418 cm^{-1}. The peak at 1751 cm^{-1}, 632 cm^{-1} in SPION/PLA-PEG/GO matches the peak at 1732 cm^{-1}, 632 cm^{-1} in GO and SPION respectively. The peak at 1624 cm^{-1} in GO matches SPION/PLA-PEG/GO spectra as depicted in Fig. 3. These spectra suggest that the drug delivery vehicle has been successfully assembled as described.

3.1.3 Loading of the Delivery Vehicle

This study loaded high molecular weight proteins by depositing them on the surface of the GO layer of the SPION/PLA-PEG/GO delivery vehicle. Hence, the larger the protein size, the better for the study. Currently, the two main proteins that many studies are focusing on are BSA and bovine hemoglobin (BhB). The average dimension of a single hemoglobin and serum albumin are 6 x 5 x 5 nm, and 7.5 x 6.5 x 4.0 nm, respectively.[28] Because BSA has larger dimensions than hemoglobin, the BSA protein was chosen as the model protein to test the drug loading capacity.

The amount of BSA adsorbed on the surface of SPION/PLA-PEG/GO is presented in Table 2. The mass of BSA adsorbed onto Fe_3O_4/PLA-PEG/GO first increases quickly due to the initial availability

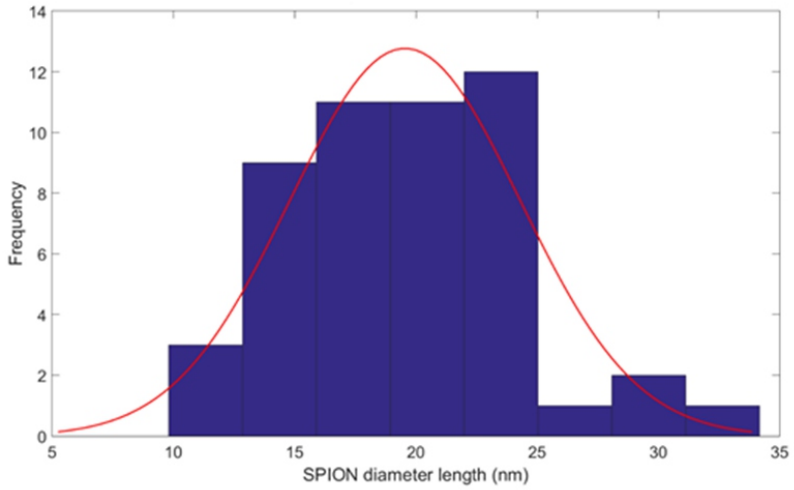

Fig. 2 The normal distribution of SPION diameter as determined using SEM software.

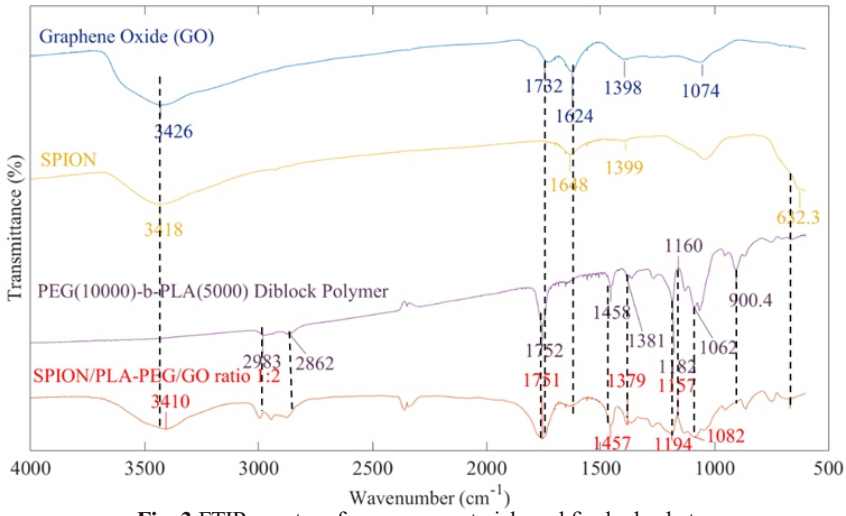

Fig. 3 FTIR spectra of precursor materials and final adsorbate.

Table 1 FTIR spectra analysis.

Spectra	Wavelength (cm^{-1})	Group	Ref.
PLA-PEG	1752	C=O	21
	2983	$-CH_3$ asymmetric stretch	21
	2862	$-CH_3$ symmetric stretch	21
	1062	C-O	21
	1458	$-CH_3$ asymmetric bend	21
	1381	$-CH_3$ symmetric bend	21
GO	3426	-OH	
	1732	C=O	18,22,23,24
	1624	C=C	18,22,24
SPION	3418 and 1648	Bending vibration of absorbed water and surface hydroxyl and O—H stretching mode	25
	900-1000	Presence of nitrate group	25
	632.3	Fe-O bonds in the crystalline lattice of Fe_3O_4	26
	1648	C=O stretching vib ration	26,27

Table 2 Drug loading capacity, percentage, and entrapment efficiency.

Average Q (mg g^{-1})	Drug Loading (%)	Entrapment Efficiency (%)
2013 ± 79 (1σ)	185.8 ± 0.0 (1 σ)	99.7 ± 0.0 (1σ)

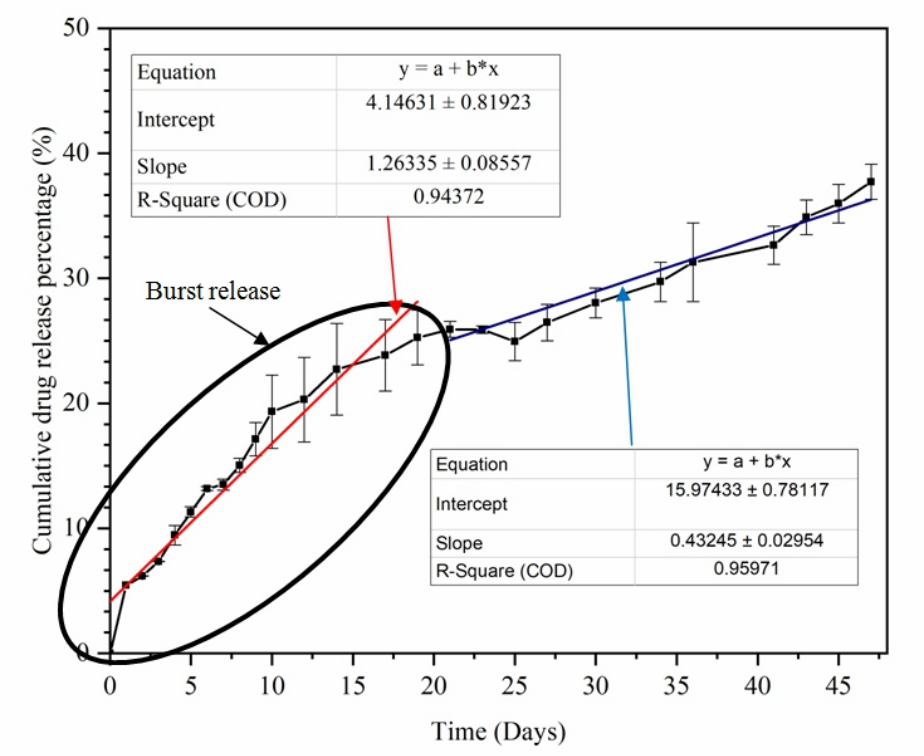

Fig. 4 *PCDRR*$_n$ versus time (1σ).

of activated graphene oxide sites due to the high concentration of BSA. After 1 minute, the BSA has occupied most of the activated sites of the GO and has reached the equilibrium state. The average Q at equilibrium is 2013 ± 79 (mg g^{-1}) (1σ).

As seen in Table 2, the average drug loading percentage is 185.8 ± 0.0% (1σ). Our model drug compound, BSA, was adsorbed onto the surface of the nanoparticles very quickly and reached the equilibrium state after 1 min.

As seen in Table 2, the entrapment efficiency percentage reached 99.7 ± 0.0% (1σ) by t = 5 min. Based on the results from Table 2, for 1 mg of SPION/PLA-PEG/GO, approximately 1.85 mg of BSA adsorbed onto the surface of the nanoparticles.

This study shows that the SPION/PLA-PEG/GO can be used as potential drug delivery vehicle for large molecules such as BSA (66 kDa).[29] This vehicle can adsorb a large quantity of drugs and has a very high entrapment efficiency in a short period of time. Comparing the drug loading capacity to previous study,[30] BSA adsorption capacity on GO is similar (200.01 mg g^{-1}). This adsorption can be ascribed to a chemisorption mechanism.[30] Moreover, because of the abundance of carboxylic acid groups, π-π* stacking interactions, hydrophilic characteristic, and different types of forces such as van der Waals interactions, electrostatic forces, hydrophobic forces, and hydrogen bonds, large amount of BSA can be adsorbed on GO.[30]

3.1.3 Release of the Delivery Vehicle

This study analyzed the release of BSA from the loaded delivery vehicle. Based on the absorbance from the UV-vis spectrophotometer, the cumulative drug release percentage is presented in Fig. 4.

The cumulative drug release percentage ($PCDRR_n$) is increasing steadily. Fig. 4 also shows that the standard deviation is small, which means that the releasing experiment is accurate and repeatable. By the end of day 47, the $PCDRR_n$ is 37.7 ± 1.4% (1σ). From day 0 to day 20, the vehicle exhibits the burst release phenomenon.[31] The $PCDRR_n$ at the end of the burst release was 25.9 ± 0.6 % (1σ). The initial burst release is possibly caused by the interaction between BSA and the graphene oxide such as a strong - stacking between BSA and SPION/PLA-PEG/GO.[31,32] According to X. Huang *et al*., burst release has not shown to understand the mechanisms of burst release in monolithic polymeric systems.[31] Another cause for the burst release is the result of a high drug concentration between the bulk solution and the BSA molecules which is attached on the GO surface.[33] Hence, X. Huang *et al*. discussed that burst release of proteins is often caused by the surface adhesion, and desorption, and the thermodynamic imbalances because the solubility of drugs and their partition coefficients affect the driving forces for release.[31] Another cause for the initial burst release of BSA during the initial release process is the quick swollen rate of the PLA-PEG, and the weak interaction between PLA-PEG matrix and BSA.[34] The burst release can be avoided by cross-linking the polymer on the GO/SPION surface.[35] Delivery vehicles that undergo burst release typically require more frequent dosing.[31] However, after 45 days this delivery vehicle only released 37.7 ± 1.4 % (1σ) of the BSA. Therefore, this delivery vehicle shows the potential for long-term release without requiring frequent dosing. This drug release model looks very similar to the release of BSA from poly (DL-lactide/glycolide, 50:50, Dupont).[36] Moreover, the BSA burst release phenomena can also be seen similarly in Sershen *et al*. study.[37] After the burst effect, the delivery vehicle sustained a near constant release rate (R^2 = 0.96). After day 47, polymer residue was suspended inside the 15 ml PBS centrifuge tube. This phenomenon suggests the degradation of the polymer. Hence, the drug release experiment was stopped after 47 days because the solution inside the centrifuge tube contained degraded polymer, and BSA. This would affect the readings of the BSA absorbance using by spectrophotometry. Further study will be required to eliminate the burst release effect.

As seen in Table 3, SPION/PLA-PEG/GO drug delivery vehicle has the highest entrapment efficiency, and one of the lowest cumulative drug release percentage.

4. Conclusions

In summary, this study has developed an easily synthesized, low-cost, and effective protein delivery carrier using SPION/PLA-PEG/GO. By using SEM, UV-Vis Spectroscopy, and FTIR, the size of the particle, the drug loading capacity, and the confirmation of the bonding of SPION, PLA-PEG, and GO were determined. This carrier has the size of 20 ± 5 nm (1σ) and a drug loading capacity of 2013 ± 79 mg g^{-1} (1σ). This study also shows that the drug loading percentage and entrapment efficiency are 185.8 ± 0.0% (1σ), and 99.3 ± 0.2% (1σ), respectively. This study also shows that the average percentage cumulative drug

Table 3 Comparison table between different types of drug delivery vehicle.

Drug Delivery Vehicle	Entrapment Efficiency (%)	Cumulative drug release percentage (%)	Reference
SPION/PLA-PEG/GO	99.7 ± 0.0 (1σ)	37.7 ± 1.4 (after 47 days) (1σ)	This study
PLGA	63.8 ± 1.4	49.8 (after 7 days)	38
PEG-PLGA	48.6 ± 1.1	71.4 (after 7 days)	38
Layer-by-layer alginate, chitosan (5 layers)	~80	~30 (after 30 days)	39
Dextran hydrogels	-	60 (after 7$\sqrt{hours}$)	40
PEG-g-chitosan hydrogels crosslinked with genipin with BSA concentrations 1000 μg/ml	-	~80 (after 40 days)	41
Alginate and montmorillonite composite beads 2% w/v	78	~40 (after 10 hours)	42

release after 47 days in vitro is 37.7 ± 1.4% (1σ), with the burst release effect in the first 20 days. This study can be researched further by testing the drug release test in in vivo.

Conflict of interest

There are no conflicts to declare.

Acknowledgements

Financial supports from the Lamar University Dan F. Smith Department of Chemical Engineering and College of Engineering are gratefully acknowledged.

References

1. E. Senkus and J. Jassem, *Cancer. Treat. Rev.,* 2011, **37**, 300.
2. W. Kucharska, M. Negrusz-Kawecka and M. Gromkowska, *Adv. Clin. Exp. Med,* 2012, **21**, 281.
3. S. Jin and K. Ye, *Recent. Pat. Anticancer Drug. Discov.,* 2013, **8**, 143.
4. G. Minotti, A. Saponiero, S. Licata, P. Menna, A. M. Calafiore, G. Teodori and L. Gianni, *Clin. Cancer. Res.,* 2001, **7**, 1511.
5. Z. Zhao, Z. Zhou, J. Bao, Z. Wang, J. Hu, X. Chi, K. Ni, R. Wang, X. Chen, Z. Chen and J. Gao, *Nat. Commun.,* 2013, **4**, 2266.
6. M. Muthiah, I. K. Park and C. S. Cho, *Biotechnol. Adv.,* 2013, **31**, 1224.
7. R. Qiao, C. Yang and M. Gao, *J. Mater. Chem.,* 2009, **19**, 6274.
8. T. Neuberger, B. Schöpf, H. Hofmann, M. Hofmann and B. von Rechenberg, *J. Magn. Magn. Mater.,* 2005, **293**, 483.
9. A. Marinin, *Synthesis and characterization of superparamagnetic iron oxide nanoparticles coated with silica. Master Thesis, Royal Institute of Technology: Stockholm, Stockholm, 2012*.
10. N. A. Alcantar, E. S. Aydil and J. N. Israelachvili, *J. Biomed.Mater. Res.,* 2000, **51**, 343.
11. A. K. Gupta and S. Wells, *IEEE T. Nanobiosci.,* 2004, **3**, 66.
12. P. Gao, M. Liu, J. Tian, F. Deng, K. Wang, D. Xu, L. Liu, X. Zhang and Y. Wei, *Appl. Surf. Sci.,* 2016, **378**, 22.
13. Y. Zhang, T.R. Nayak, H. Hong and W. Cai, *Nanoscale,* 2012**,** 3833-3842.
14. E. K. Wujcik and C. N. Monty, *Wires. Nanomed. Obi.*, 2013, ***5***, 233-249.
15. D. W. Boukhvalov, *Phys. Chem. Chem. Phys.s,* 2010, **12**, 15367.
16. A. Angelopoulou, E. Voulgari, E. K. Diamanti, D. Gournis and K. Avgoustakis, *Eur. J. Pharm. Biopharm.,* 2015, **93**, 18-26.
17. I. J. Bruce, J. Taylor, M. Todd, M. J. Davies, E. Borioni, C. Sangregorio and T. Sen, *J. Magn. Magn. Mater.,* 2004, **284**, 145-160.
18. Y. Huang, Y. Wang, Q. Pan, Y. Wang, X. Ding, K. Xu, N. Li and Q. Wen, *Anal. Chim. Acta,* 2015, **877**, 90.
19. S. Papadimmitriou and D. Bikiaris, *J. Control. Release,* 2009, **138**, 177-184.
20. S. J. Kiprono, M. W. Ullah and G. Yang, *Appl.Microb. Cell Phys.*, 2017, **102**, 933-944.
21. B. Chieng, N. Ibrahim and W. Yunus, M. Hussein, *Polymers,* 2013, **6**, 93.
22. M. Fu, Q. Jiao, Y. Zhao and H. Li, *J. Mater. Chem. A,* 2014, **2**, 735.
23. P. Lian, X. Zhu, S. Liang, Z. Li, W. Yang and H. Wang, *Electrochim. Acta,* 2010, **55**, 3909.
24]. S. Gurunathan, J. W. Han, J. H. Park, E. S. Kim, Y. J. Choi, D. N. Kwon and J. H. Kim, *Int. J. Nanomed.,* 2015, **10**, 4203-4222.
25. S.W. Hwang, A. Umar, G. N. Dar, S.H. Kim and R. I. Badran, *Sens. Lett.*, 2014, **12**, 1-5.
26. J. Lopez, F. González, F. Bonilla, G. Zambrano and M. Gómez, *Rev. Latinoam. Metal. Mater.,* 2010, **30**, 60-66.
27. M. D. Adhikari, S. Mukherjee, J. Saikia, G. Das and A. Ramesh, *J. Mater. Chem. B,* 2014, **2**, 1432.
28. H. P. Erickson, *Biol. Proced. Online,* 2009, **11**, 32.
29. J.J. Babcock and L. Brancaleon, *Int. J. Biol. Macromol.*, 2014, **53**, 42-53.
30. H. Zhang, Z. Zhu, Y. Wang, Z. Fei and J. Cao, *Appl. Surf. Sci.*, 2018, **427**, 1019-1029.
31. X. Huang, C.S. Brazel and *J. Control. Release*, 2001, **73**, 121-136.
32. H. Hu, C. Tang and C. Yin, *Mater. Lett.*, 2014, **125**, 82-85.
33. T. Kumeria, M. Bariana, T. Altalhi, M. Kurkuri, C.T. Gibson, W. Yang and D. Losic, *J. Mater. Chem. B*, 2013, **45**, 6302-6311.
34. X. Zhao, X. Zou and L. Ye, *J. Ind. Eng. Chem.,* 2017, **49**, 36-45.
35. X. Ma, H. Tao, K. Yang, L. Feng, L. Cheng, X. Shi, Y. Li, L. Guo and Z. Liu, *Nano Res.,* 2012, **5**, 199-212.
36. H. T. Wang, E. Scmitt, D. R. Flanagan and R. J. Linhardt, *J. Control. Release*, 1991, **17**, 23-31.
37. S. R. Sershen, S. L. Westcott, N. J. Halas and J. L. West, *J. Biomed. Mater. Res.*, 2000, **51**, 293-298.
38. Y. P. Li, Y. Y. Pei, X. Y. Zhang, Z. H. Gu, Z. H. Zhou, W. F. Yuan, J. J. Zhou and X. J. Gao, *J. Control. Release*, 2001, **71**, 203-211.
39. Z. S. Haidar, R.C. Hamdy and M. Tabrizian, *Biomaterials*, 2008, **29**, 1207-1215.
40. W. E. Hennink, O. Franssen, W. N. E. van Dijk-Wolthuis and H. Talsma, *J. Control. Release*, 1997, **48**, 107-114.
41. N. Bhattarai, H. R. Ramay, J. Gunn, F. A. Matsen and M. Zhang, *J. Control. Release,* 2005, **103**, 609-624.
42. H. Kaygusuz and F. B. Erim, *React. Funct. Polym.*, 2013, **73**, 1420-1425.

